Alignment and Characterization of Carbon Nanotubes on Photolithographically Patterned Electrodes

by

Hyungbin Son

Submitted to the Department of Electrical Engineering and Computer Science

in Partial Fulfillment of the Requirements for the Degrees of

Bachelor of Science in Electrical Science and Engineering

and Master of Engineering in Electrical Engineering and Computer Science

at the Massachusetts Institute of Technology

May 20, 2004
[June 2004]

Author .....
Department of Electrical Engineering and Computer Science
May 20, 2004

Certified by .....
Mildred S. Dresselhaus
Thesis Supervisor

Accepted by .....
Arthur C. Smith
Chairman, Department Committee on Graduate Thesis

Alignment and Characterization of Carbon Nanotubes on Photolithographically Patterned Electrodes

by

Hyungbin Son

Submitted to the
Department of Electrical Engineering and Computer Science

May 20, 2004

in Partial Fulfillment of the Requirements for the Degrees of
Bachelor of Science in Electrical Science and Engineering
and Master of Engineering in Electrical Engineering and Computer Science

ABSTRACT

The goal of this work is to make an (n,m) assignment for individual suspended single wall carbon nanotubes (SWNTs) based on the measurements of their Raman Radial Breathing Modes and electron transition energies E_{ii} based on Raman spectroscopy. The suspended SWNTs are grown on a photolithographically defined electrode pattern, which is designed so that suspended SWNTs are grown at known locations with known directions. The suspended SWNTs are then characterized by atomic force microscopy (AFM), scanning electron microscopy (SEM), and Raman spectroscopy. Finally, the information on the diameter distribution and the energy of the electronic transitions of the resonant suspended SWNTs obtained from Raman spectroscopy is compared to other published works to make (n,m) assignments of a number of suspended SWNTs.

Thesis Supervisor: Mildred S. Dresselhaus
Title: Institute Professor of Physics and Electrical Engineering

Acknowledgments

First of all, I thank my advisor Professor Mildred S. Dresselhaus for her guidance and support throughout the thesis work. She is extremely busy but readily available, makes me work hard but does not stress me, lets me do what I wish to do but guides me to do the right thing, and makes me feel that her group is my group. I am grateful that I joined this group.

I also thank my parents back in Korea for their support throughout my period of study here at MIT, not to mention about earlier period of my life. They are not scientists nor engineers, but taught me to have a solid mind.

I express my gratitude to my group members, Gene Dresselhaus, George, Grace, Daniel, Steve, Victor, Nasser, Yuki, Ming, and Oded for warm welcome and valuable discussions.

Gene and Oded helped me to get myself acquainted with the group. Also, when I'm locked out of my office or lab, they were the ones who open the door for me (thank you!).

George helped me a lot with any theory question I had. He also had a library of related published papers, which I could get any time I want (he stays in his office all the time).

Grace helped me to start up with my experiments. She taught me how to perform Raman spectroscopy and to analyze the Raman spectra.

Yuki studied the growth of SWNTs by herself and helped me greatly with stabilizing the growth process.

Steve also helped me with the growth of SWNTs. When I was starting to grow SWNTs, I obtained the recipe for the gas composition and the catalyst from him.

Daniel is my officemate. He likes to talk and makes me feel like home in my office. For example, when I have strange ideas about experiments, he is the one I can talk to.

Ming, although his research topic is not related to mine, is a extraordinarily humorous student and it is always fun to talk with him. I hope that his research

topic gets related to mine so that we can work together.

Nasser is a very talkative undergraduate student. Working as a graduate student, I tend to become deaf to all stories around the campus. He was the source of gossip and brought delight to my graduate life.

Victor is an enthusiastic physics student and is very excited about quantum physics of electron spins. It was a joy to listen to his idea on how to use SWNTs to demonstrate coherent electron spins.

Eduardo is a bright student visiting from Brazil and working closely with me. I thank him for useful discussions on the band structure and optical transitions of SWNTs and experimental setup.

I appreciate Ernesto Joselevich's help with the catalyst preparation. Growing small diameter SWNTs would have been impossible without his help.

I acknowledge support under NSF Grants DMR-01-16041 and INT 00-00408. I cannot say too much words of gratitude for Intel for giving us resources to enable us to do this kind of work. This work made use of MRSEC Shared Facilities supported by the National Science Foundation under Award Number DMR-0213282 and NSF Laser Facility grant #CHE-011370.

Contents

1 Introduction **9**

2 Sample preparation **13**

2.1 Design and Fabrication of electrodes 15

2.2 Growth of SWNTs using CVD 16

3 Sample characterization **19**

3.1 AFM characterization 19

3.2 SEM characterization 21

4 Raman spectroscopy **27**

5 Discussion **35**

Chapter 1

Introduction

A single wall carbon nanotube (SWNT) is a new form of carbon, whose atomic arrangement is equivalent to a graphite sheet rolled into a cylinder in a seamless way [24]. The electronic band structure of a SWNT has unique properties, which are useful for a variety of applications [4]. Because of the one dimensionality of SWNTs, there exist singularities in the density of states, called Van Hove singularities. The band structure is determined by the geometric configuration of the SWNT [24]. The band gap can be varied by changing the geometric configuration to make the nanotube either metallic or semiconducting. In the case of a semiconducting SWNT, the band gap corresponds to the energy gap between the two Van Hove singularities in the valence and conduction bands closest to the Fermi level.

Van Hove singularities in SWNTs have enabled the observation of various interesting photophysics phenomena, two of the most important ones being Raman spectroscopy [8] and band gap photoluminescence measurements [19, 1, 17]. Raman spectroscopy measurements have been performed on various forms of SWNTs, including bundled SWNTs [23], an individual SWNT on a silicon and silicon oxide (Si/SiO_2) substrate [9, 7], suspended SWNTs [12], the inner wall of a double wall carbon nanotube (DWNT) [14], and SWNTs wrapped with various surfactants and DNA molecules [1, 6, 3]. Band gap photoluminescence has been observed from suspended SWNTs, SWNTs wrapped with sodium dodecyl sulfate (SDS) and DNA molecules [17, 1, 3]. Furthermore, very narrow linewidths for the Raman radial breathing modes

(RBM) have been observed on the inner wall of a DWNT [21] and sharply peaked, strong band gap photoluminescence and enhanced Raman signals have been obtained from suspended SWNTs [17, 14]. These results suggest that both suspended SWNTs and the inner wall of a DWNT are under a highly unperturbed environment [21] and, with selected external perturbations, are promising candidates for optical device applications [10]. For example, the inner wall of a DWNT can be perturbed by a light resonant with its electronic transition energy.

However, it remains a challenge to assign the energy gaps (E_{ii}) and Raman spectral features to the corresponding SWNT diameter and chirality. This link is essential for understanding the underlying physics of a SWNT, its electronic band structure and vibrational modes, and this link is also important in practice, since Raman spectroscopy and photoluminescence are commonly used to characterize SWNTs. Although the (n,m) index assignments, which uniquely identify one nanotube from another, have been made on SWNTs wrapped with SDS, prior studies have been limited to the RBM features of the Raman spectra. Thus far, the analysis of SDS wrapped SWNTs has only been carried out on an ensemble of SWNTs rather than on individual SWNTs [1, 6]. Furthermore, no systematic Raman studies have been carried out on suspended SWNTs due to various experimental difficulties, one of them being that SWNTs tend to bundle up when they are placed too close to one another, disabling studies to be made on 'bulk' suspended SWNTs. Thus far, the published photoluminescence data is limited to only a small number of (n,m) suspended SWNTs [17], and thus the assignment of the energy gap to the diameter and chirality of suspended SWNTs is not clear at this point.

The motivation of this thesis is to make an assignment for the Raman RBM modes and the energy gaps of suspended SWNTs. SWNTs studied in this thesis are suspended between two electrodes and the preparation methods are described in Chapter 2. The electrode pattern is designed so that suspended SWNTs are grown at known locations with known directions, and an individual SWNT can be resolved from other SWNTs and can be located easily. Thus, multiple characterization techniques with different conditions can be applied to the same SWNT. In Chapter 3, the suspended

SWNTs are characterized by atomic force microscopy (AFM), scanning electron microscopy (SEM), and Raman spectroscopy, as described. The AFM study enables the estimation of the diameter distribution of SWNTs on a flat surface. The SEM study reveals the density, location and alignment of SWNTs. In Chapter 4, the suspended SWNTs are characterized by Raman spectroscopy, which gives information on the diameter distribution and the energy gaps of the resonant suspended SWNTs, which is necessary to make unique (n,m) assignments for the SWNTs. In Chapter 5, the information on the diameter distribution and the energy gaps of the resonant suspended SWNTs obtained from Raman spectroscopy is compared to other published works to make an (n,m) assignment of suspended SWNTs.

Chapter 2

Sample preparation

To be able to characterize suspended SWNTs, it is essential to prepare high quality suspended SWNTs, i.e. defect-free, mostly suspended, reasonably long and mostly single walled. Furthermore, knowing the directional alignment and the locations of the suspended SWNTs and being able to address them repeatedly will enable various interesting experiments, such as Raman spectroscopy with polarization and Raman spectroscopy on the same suspended SWNT with different temperatures, chemical environments and laser lines.

Previous works on preparing suspended SWNT used silicon nanopillars [12], pairs of Pt/W metal gates supported by a Si_3N_4 film [2], and polysilicon gates with electric field [26]. The suspended SWNTs prepared on silicon nanopillars are relatively short (500nm in length), not aligned in any single direction and not addressable as the pattern is too small to be seen by an optical microscope (Figure 2-1 (a)) [12]. The suspended SWNTs prepared on Pt/W metal gates are not well suited for resonant Raman spectroscopy, because of charge transfer from the electrodes to the nanotubes. Since the pattern is fabricated by electron-beam lithography, there is some difficulty in preparing a sufficient number of metal gates for the number of SWNTs required for resonant Raman spectroscopy (Figure 2-1 (b)) [2]. The suspended SWNTs grown on the polysilicon gates are not addressable (Figure 2-1 (c)) [26], since they are grown on parallel electrodes and there is no marker on the electrodes.

A new approach using conventional silicon technology is employed and the pattern

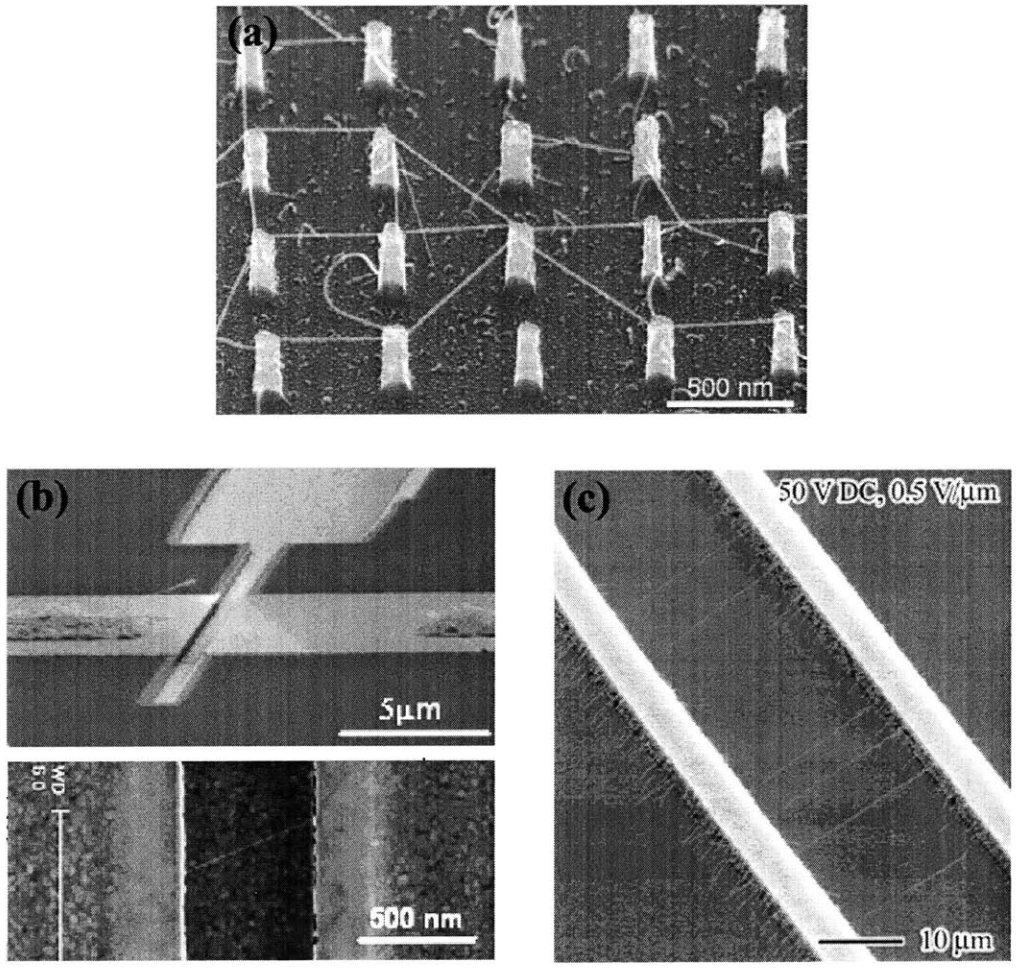

Figure 2-1: Previous works on growing suspended SWNTs, (a) on silicon nanopillars, (b) on Pt/W electrodes patterned by electron-beam lithography, and (c) on parallel polysilicon electrodes.

is designed so that the suspended SWNTs are long (1~4um in length), well aligned, and addressable.

2.1 Design and Fabrication of electrodes

The electrodes serve as both electrical contacts and as elevated structures for suspending the SWNTs. The electrode pattern is designed so that suspended SWNTs are grown at known locations with known directions. A suspended SWNT is locatable within 1um accuracy by an optical microscope and by SEM (scanning electron microscopy). The electrodes are fabricated using standard silicon technology: chemical vapor deposition (CVD) of polysilicon films, thermal growth of SiO_2 films, and photolithography. In contrast to electron beam lithography, a large-scale device can be made by photolithography: about fifty thousand pairs of electrodes are fabricated on a single 1cm by 1cm sample.

The cross section of the electrode design is shown in Figure 2-2 (a) to illustrate how an elevated structure can support a suspended SWNT. Polysilicon electrodes are deposited on top of a 1um-thick film of SiO_2. A trench is introduced between the electrodes to provide both electrical isolation and a suspended structure, as explained below. Furthermore, an electric field can be applied between the electrodes to facilitate growth of the suspended SWNTs growing between the electrodes [20] and to align them [26].

The top view of the electrode design is shown in Figure 2-2 (b) to illustrate how the location and the direction of suspended SWNTs can be controlled by the electrode pattern. The narrow trenches are 1~4um wide, so that a high electric field on the order of 10^6(V/m) can be applied easily between the electrodes. The wide trenches are 10um wide so that the electric field in the wide trench region is significantly weaker than in the narrow trench region. A high electric field is known to enhance the growth rate of SWNTs and to align them [20, 26]. Moreover, by controlling the maximum length of SWNTs, one can guarantee that there is no suspended SWNT growing across the wide trench and that all the growth occurs in the narrow trench

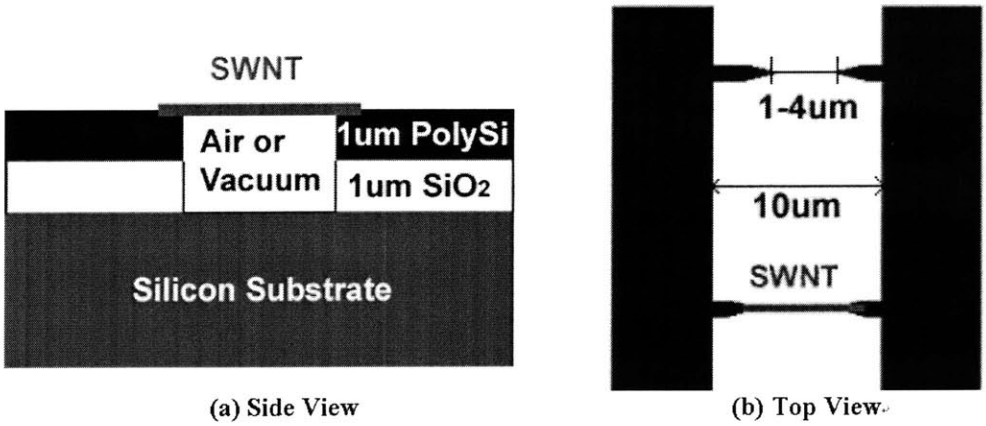

Figure 2-2: Schematic of suspended SWNTs between electrodes.

region, as shown in Figure 2-2 (b).

The actual growth of the electrode structures for subsequent use for preparing suspended SWNTs is as follows. Conventional silicon technology is employed to fabricate the polysilicon electrodes. A 1um-thick silicon oxide film is grown on 6-inch wafers by a wet thermal oxidation process at 1050°C. On top of the silicon oxide film, a 1um-thick polysilicon film is deposited using CVD. Then 1um of photoresist film is patterned using the Hg I-line (365nm). The trench region of the polysilicon film and the silicon oxide film is etched by a reactive ion etch using HBr and CF_4, respectively, and the photoresist is removed by an oxygen plasma ash method. For better signal to noise ratio when doing Raman spectroscopy, some samples are prepared with a deeper trench into the silicon substrate, which is etched by using SF_6.

2.2 Growth of SWNTs using CVD

The SWNTs are grown directly on the sample by methane CVD [15]. The catalyst particles needed for catalyzing the SWNT growth are the iron nanoparticles prepared by mixing iron (III) nitrate and sodium hydrogen carbonate in aqueous solution [11]. Samples were prepared both with and without applied electric fields between the electrodes.

The SWNTs are grown directly from randomly deposited iron nanoparticles on the

sample. The iron (III) oxide nanoparticles suspension is prepared by mixing 50.5mg of iron(III) nitrate, 21mg of sodium hydrogen carbonate, and 50mL of deionized water and stirring the mixture for 1~4hrs. To deposit the catalyst particles, the samples are dipped in the catalyst suspension for 1~5 minutes and then thoroughly washed with ethanol and finally blown dried with nitrogen at room temperature. The stirring time and the dipping time were correlated with the diameter distribution and the density of the SWNTs, respectively, which is discussed in chapter 3. After the catalyst particle deposition, the samples are brought into a one-inch tube furnace. First of all, the samples are heated from room temperature to 800~900 °C linearly in 30 minutes with 50cm^3/min of Hydrogen and 100cm^3/min of Argon flow, so that the iron oxide nanoparticles are reduced to iron nanoparticles. Then the samples are kept at the final temperature for 5~15 minutes with 100cm^3/min of methane, 50cm^3/min of Hydrogen, and 100cm^3/min of Argon flow. After the growth is completed, all the gases other than Argon are turned off and the samples are cooled down to room temperature. Both fast and slow cooling conditions are tested: the sample cools down slower if all the gas is turned off and the furnace is kept closed and it cools down faster if the argon flow is kept on and the furnace is opened. However, no difference in the sample in terms of the density, the alignment and the diameter of the SWNTs that are grown is found between the two cooling conditions. No difference in the oxygen adsorption between the two cooling conditions is expected since the sample is cooled down to room temperature in Argon gas before any air gets in.

Chapter 3

Sample characterization

The samples are characterized by AFM and by SEM. The AFM study reveals the diameter distribution and the density of SWNTs growing on a flat surface. The SEM study reveals the location, the density and the alignment of both SWNTs growing on a flat surface and suspended SWNTs growing between trenches. Carbon nanotubes ranging from diameter 0.5nm to 6nm are found by the AFM study. However, the accuracy of the diameter measured by the AFM study is about 0.2nm and serves only as a quick way to characterize the sample before performing the Raman spectroscopy measurements. The diameter distribution is correlated to the stirring time of the iron (III) oxide nanoparticle suspension. The SEM study confirms that the samples grown with an applied field between the electrodes has well aligned tubes across the narrow trenches and few tubes growing across the wide trenches.

3.1 AFM characterization

SWNTs growing on a silicon oxide and silicon substrate (Si/SiO_2 substrate) are characterized by AFM. Two types of substrates are prepared: one is prepared by growing a thin film of SiO_2 by exposing a silicon substrate to air at room temperature, and the other is prepared by growing a 1um-thick SiO_2 film by a wet thermal oxidation process at 1050°C. As there is no way to directly image the diameter of suspended SWNTs in the samples that were prepared, the AFM study on SWNTs on a Si/SiO_2

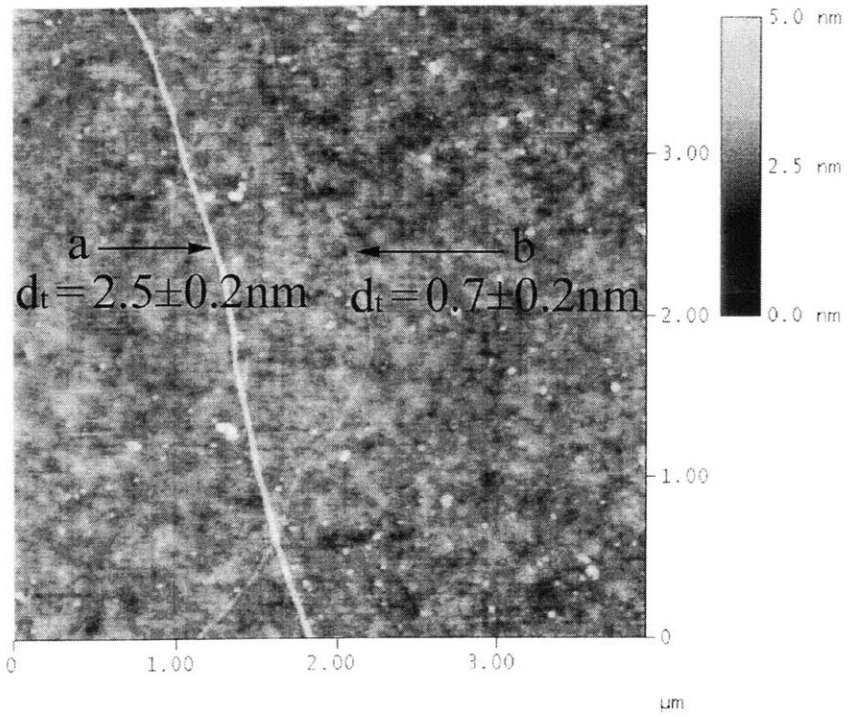

Figure 3-1: A typical image of SWNTs growing on a Si/SiO_2 substrate. The scale bar on the right side indicates the height of the image. Nanotube (a) has a diameter (d_t) of 2.5±0.2nm and possibly is a small bundle of SWNTs or a DWNT. Nanotube (b) has a diameter of 0.7±0.2nm and is a SWNT.

substrate serves as a guide for controlling the diameter of the suspended SWNTs. AFM images give information about the approximate diameter, the length, and the density of SWNTs in the region under inspection. The length and the density of SWNTs, however, can be obtained more easily from the SEM study. Thus, the AFM study was focused on the diameter distribution of SWNTs and on establishing any dependence there might be on the growth conditions. Figure 3-1 shows a typical AFM image of two SWNTs growing on a Si/SiO_2 substrate. By comparing the scale bar and the image of SWNTs, the diameter of the SWNTs can be determined within about 0.2nm accuracy. AFM images taken from both the native oxide film and 1um-thick oxide film grown by a wet thermal oxidation process at 1050°C are examined and no difference is found in terms of the diameter and the length of the SWNTs.

The only growth condition that is found to have any significant correlation with the diameter distribution of SWNTs is the stirring time. As the stirring time of the

catalyst suspension increases, the size of iron (III) oxide nanoparticle precipitating in the suspension is expected to increase. Moreover, the diameter of SWNTs is positively correlated to the size of the catalyst particles [18]. Figure 3-2 demonstrates this expected diameter dependency of SWNTs on the stirring time of the catalyst. Three samples were prepared by growing SWNTs on a Si/SiO_2 substrate at 900°C with stirring times of 1.5hrs, 3hrs, and 4hrs, respectively. The dipping time was fixed at 5 minutes. About ten to twenty SWNTs are characterized from each sample and the diameter distribution for each sample is plotted in Figure 3-2. As the diameter distribution does not follow a simple distribution, the mean diameter and the standard error in the mean are calculated and shown for each sample. SWNTs with diameters down to 0.4nm is observed. However, SWNTs with such a small diameter are hard to make and possibly unstable, and the accuracy of the diameter measured by the AFM measurements is about 0.2nm. In Figure 3-3, the mean diameter is plotted with the standard deviation of the diameter distribution (large error bar) and the standard error in the mean diameter (small error bar). The positive correlation between the stirring time and the mean diameter is clearly seen in both plots. The typical diameter of SWNTs on a sample prepared with the stirring time of 48hrs was about 5nm.

SWNTs grown at 800°C were not examined carefully by AFM measurements. However, Raman spectroscopy measurements in Chapter 4 show that a sample prepared at a growth temperature of 800°C and with a stirring time of 4hrs has SWNTs with diameters ranging from 0.9nm to 1.7nm. A more systematic study on the dependence of the diameter of SWNTs on the growth temperature would be an interesting topic for future work.

3.2 SEM characterization

SEM is a convenient tool to characterize the density, the length and the alignment of SWNTs. It is also powerful in locating suspended SWNTs as the imaging can be done at an oblique angle. Thus, the SEM study focuses on characterizing the dependence of the density, the location and the alignment of suspended SWNTs on the growth

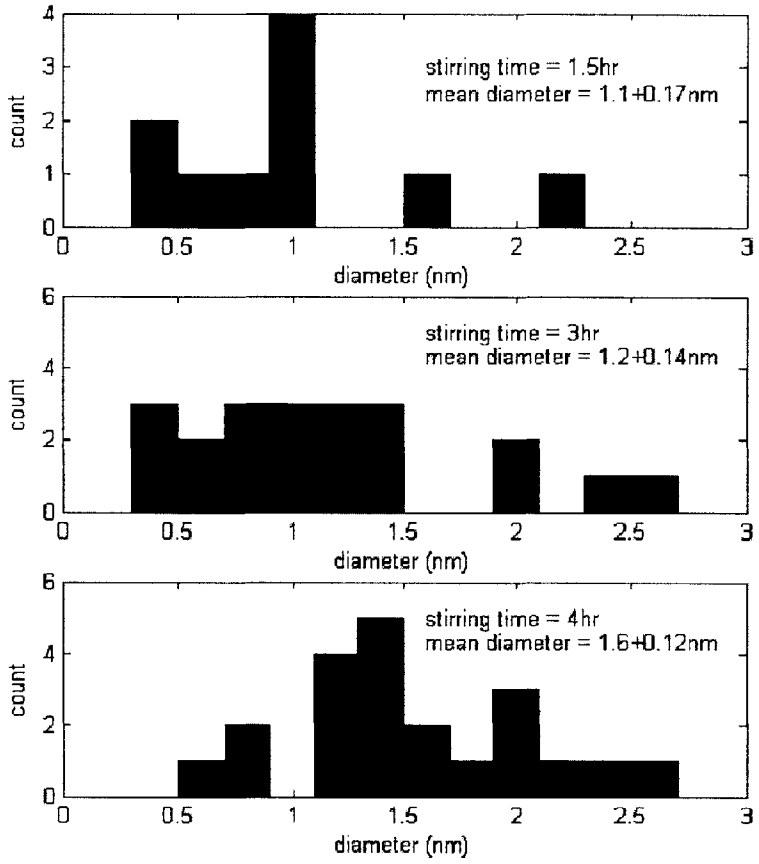

Figure 3-2: The diameter distribution (obtained by AFM measurements) of SWNTs growing on a Si/SiO_2 substrate varying the stirring time of the catalyst suspension. The mean diameter and the standard error in the mean, which is obtained from dividing the standard deviation by the square root of the number of data points, are shown for each sample. The accuracy of the diameter is about 0.2nm.

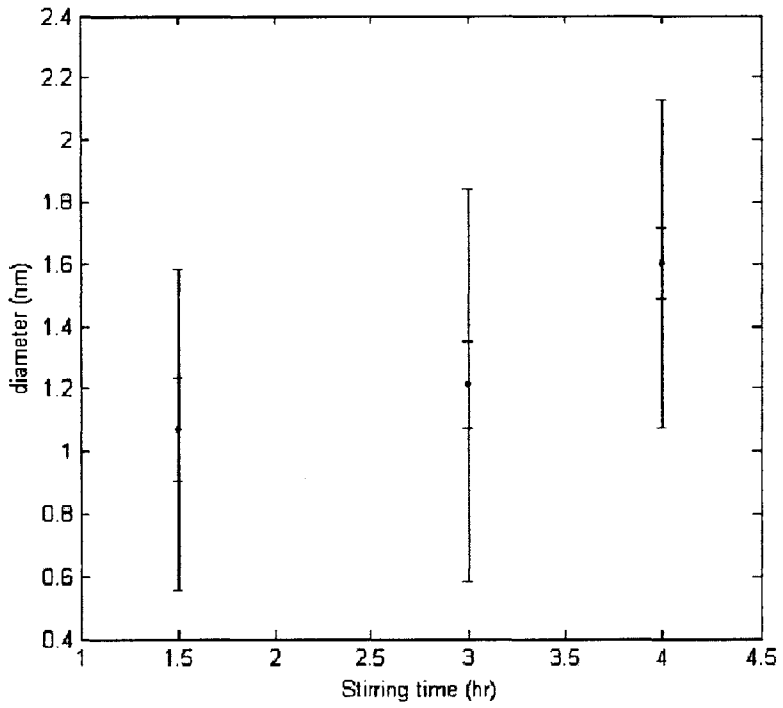

Figure 3-3: The diameter distribution of SWNTs growing on a Si/SiO_2 substrate versus the stirring time of the catalyst suspension. The mean diameters are shown as dots, the number normalized standard deviations are shown as the small error bars, and the standard deviations of the diameter distribution are shown as the large error bars.

conditions. SEM images show that the dipping time of the sample in the catalyst suspension is relevant to the density of the suspended SWNTs. An applied electric field between the electrodes aligns the suspended SWNTs between the electrodes and, when combined with selected growth conditions, such as low temperature and small dipping time, increases the selectivity of suspended SWNT growth to the narrow trench regions.

Figure 3-4 (a) is an SEM image of SWNTs grown in the 2um narrow trench regions without an applied electric field and is taken at about 30,000 times magnification. The sample was prepared under the following growth conditions: the stirring time was 4 hours, the dipping time was 5 minutes, and the growth temperature was 900°C. Figure 3-4 (b) is an SEM image of SWNTs grown in the 4um narrow trench region and the 10um wide trench region of the same sample with an applied potential of 1.5V and is taken at 9,000 times magnification. At 9,000 times magnification, which is the highest magnification that is needed to image the wide trench region, not all the SWNTs can be seen in the image and it is hard to resolve SWNTs that are as close together as in Figure 3-4 (a). However, close inspection shows that most of the suspended SWNTs are in the narrow trench region, regardless of the applied electric field and the size of the trench, except for a few SWNTs connecting the spikes and the walls of the same electrode.

The position of electrodes in the narrow trench region allows the suspended SWNTs to grow only between the spikes of the electrodes. However, without an applied electric field, SWNTs connect the two electrodes rather arbitrarily: some SWNTs connect the electrodes diagonally and some SWNTs are curved as shown in Figure 3-4 (a). With an applied electric field, the SWNTs are straight and are well aligned, as shown in Figure 3-4 (b).

About 5 to 10 tubes are found in the 2um narrow trench region and bundles of a few SWNTs can be found easily. To reduce the number of bundled SWNTs, the density of the SWNTs was lowered by decreasing the dipping time to 1 minute. Furthermore, to eliminate the SWNTs connecting the spikes and the walls of the same electrode, a lower growth temperature of 800°C was used. Figure 3-4 (c) shows the

SWNTs growing in the 2um narrow trench region of the sample prepared under the following conditions: the stirring time was 4 hours, the dipping time was 1 minute, and the growth temperature was 800°C. There are significantly fewer SWNTs growing between the electrodes and most of the SWNTs are straight. A few bundled SWNTs are found, but the fraction of bundled SWNTs in this sample is smaller than in the sample shown in Figure 3-4 (a). A close inspection shows that there are virtually no SWNTs growing except in the narrow trench region.

Compared to previous works on growing suspended SWNTs as shown in Figure 2-1, the work in Chapter 2 and 3 shows that the following has been done. First, a large-scale device with enough suspended SWNTs for resonance Raman spectroscopy is made. Second, the suspended SWNTs growing on the device are well aligned and addressable. Third, the suspended SWNTs grow only at selected locations, that is, in the narrow trench regions. Finally, the approximate tube diameter distribution is known and the diameters are small enough for Raman spectroscopy.

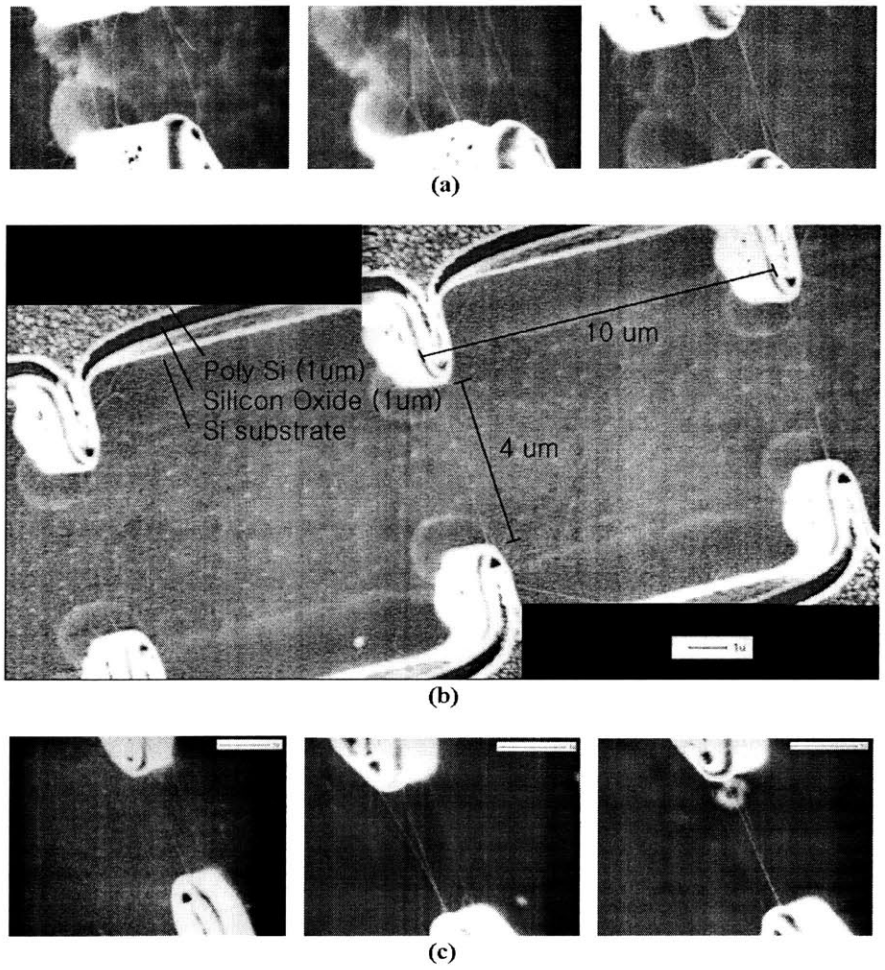

Figure 3-4: SEM images of suspended SWNTs grown under varying conditions and taken with an acceleration potential of 3kV. (a) SWNTs growing in the 2um narrow trench region of a sample prepared with the stirring time of 4 hours, the dipping time of 5 minutes, and the growth temperature of 900°C. No electric field was applied between the electrodes. (b) SWNTs growing in the 4um trench region of the same sample as in (a), but with 1.5V potential applied between the electrodes. (c) SWNTs growing in the 2um narrow trench region of a sample prepared with the stirring time of 4 hours, the dipping time of 1 minute, the growth temperature of 800°C, and with 1.5V potential applied between the electrodes.

Chapter 4

Raman spectroscopy

Raman spectroscopy measurements have been performed on suspended SWNTs at room temperature using Hololab 5000R Modular Research Raman Spectrometer with Microprobe by laser lines of E_{laser} = 1.58eV and 2.41eV. Trapezoidal and triangular lineshapes for the RBM bands are observed, which indicates that the linewidths of the RBM bands are comparable to or smaller than the instrumental resolution. The RBM band intensities obtained from suspended SWNTs are enhanced compared to the RBM bands obtained from SWNTs on a silicon oxide surface. The temperature of the suspended SWNTs did not increase even when taken with the highest available power laser of 20mw focused on them. A normalized anti-Stokes to Stokes intensity ratio down to 0.1 is observed, which suggests that the resonance window is narrow.

Figure 1 shows a typical Raman spectrum taken from a suspended SWNT with E_{laser} = 2.41eV. The signals from most bands are very strong compared to the silicon feature at 303cm^{-1}, except for the D-band, which is highly suppressed due to the lack of interaction between the suspended SWNT and the environment. All the Raman features such as the RBM band, the G-band, the G'-band, and the D'-band contain useful information, such as their dependence on the diameter and the environment of the SWNT and its interaction with neighboring SWNTs. However, this work focuses on the RBM band, since it gives the most reliable information on the diameter and the E_{ii} of the SWNT.

Figure 4-2 shows the anti-Stokes and Stokes RBM bands of the Raman spectra

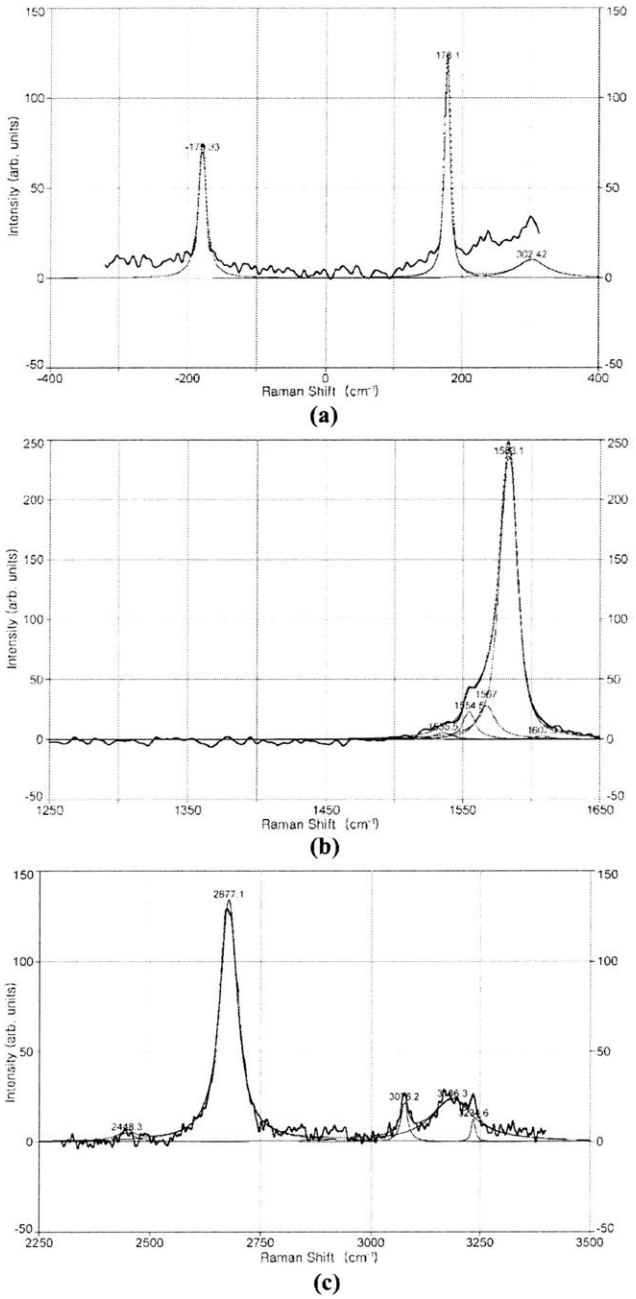

Figure 4-1: (a) The RBM band, (b) the D-band*, the G-and, and (c) the G'-band and the D'-band of the Raman spectrum of a suspended SWNT taken with E_{laser} = 2.41eV. * The D-band is highly suppressed and does not show up at Raman shifts in the range 1300$\sim$1350cm^{-1}.

taken from a suspended SWNT in a single scan with E_{laser} = 1.58eV. The peaks at -270cm^{-1} and 270cm^{-1} represent the anti-Stokes and the Stokes part of the RBM bands, respectively. The peaks at -303cm^{-1} and 303cm^{-1} are the Raman features of the silicon oxide substrate. Since the peakshapes are significantly different from the Lorentzian lineshape, the lineshapes are analyzed by deconvolving with the instrument function, which is a Gaussian or a triangular function. However, because the resolution of the spectrometer, which is about 1.5cm^{-1}, is comparable to the width of instrument function, which is about 1.5cm^{-1}, using a Gaussian or a triangular instrument function gave essentially the same numerical result for the peak frequency and the full width half magnitude (FWHM) linewidth. In fact, deconvolving the peak by a Gaussian function and fitting it to a Lorentzian function is equivalent to fitting it to the convolution of Gaussian and the Lorentzian functions. However, the second method is numerically more stable because deconvolving by a Gaussian function tends to amplify the noise in the spectrum and does not require any sort of noise filtering. Thus, the peaks are fitted to the Voigt function $f(\omega)$, which is the convolution of a Gaussian and a Lorentzian function:

$$f(\omega) = A\frac{\int_{-\infty}^{\infty} \frac{exp(-t^2)}{\frac{\Gamma^2}{2\sigma^2}+(\frac{\omega-\omega_0}{\sqrt{2}\sigma}-t)^2}dt}{\int_{-\infty}^{\infty} \frac{exp(-t^2)}{\frac{\Gamma^2}{2\sigma^2}+t^2}dt} \tag{4.1}$$

, where A is the amplitude of the peak, σ is the Gaussian linewidth (standard deviation), Γ is the Lorentzian linewidth (half width half maximum intensity), and ω_0 is the center frequency. The linewidths for Gaussian and the Lorentzian components are shown in the plot. The linewidths for the anti-Stokes sides are not shown because the linewidths determination usually are not reliable due to the smaller signal strength of the anti-Stokes side compared with the signal strength of the Stokes side.

Figure 4-3 demonstrates an example of a low anti-Stokes to Stokes intensity ratio (I_{AS}/I_S) of the RBM bands. To get the temperature of the suspended SWNTs under the laser illumination, the I_{AS}/I_S ratio was measured on a suspended SWNT by varying the laser power from 5mw to 20mw. The ratio remained constant at all laser

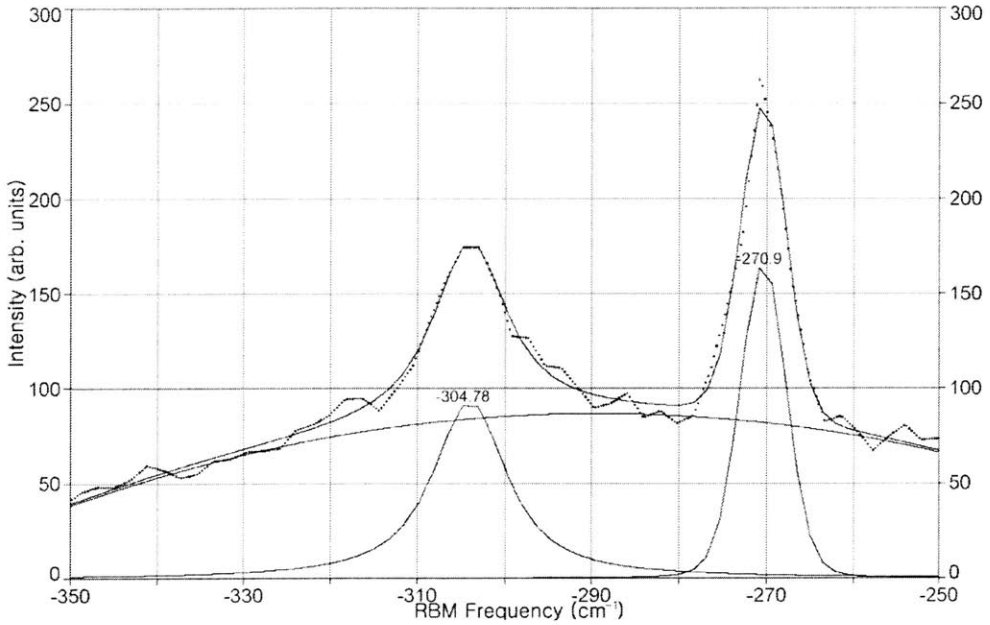

(a) Anti-Stokes RBM mode spectrum of a suspended SWNT

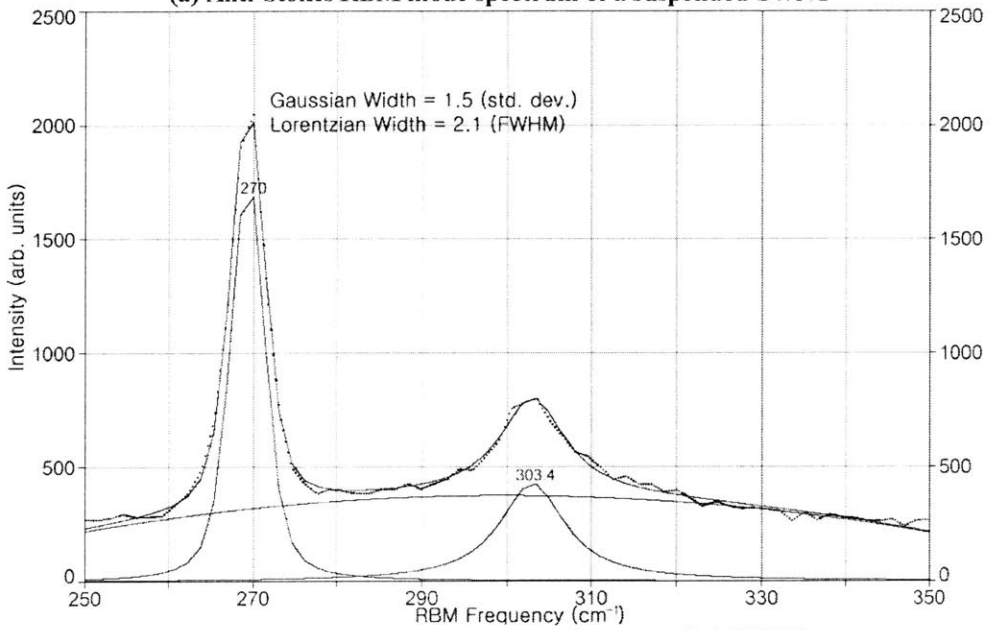

(b) Stokes RBM mode spectrum of a suspended SWNT

Figure 4-2: The anti-Stokes and Stokes RBM bands of the Raman spectra taken from a suspended SWNT simultaneously with $E_{laser} = 1.58$eV, demonstrating a narrow linewidth.

powers, which indicates that the temperature of the suspended SWNT remains at room temperature. Thus, the anti-Stokes intensity is normalized by the Boltzmann factor at 300K, which is used to calculate the temperature-normalized anti-Stokes to Stokes intensity ratio (normalized I_{AS}/I_S). The normalized I_{AS}/I_S of the suspended SWNT shown in Figure 4-3 is 0.09. Such a low ratio indicates that the resonance window is narrow [6] and that the corresponding E_{ii} is close to the laser energy (E_{laser}) minus the phonon energy (E_{ph}), which is 1.55eV.

Figure 4-4 shows the Raman spectra taken from SWNTs on a Si/SiO_2 substrate [9]. Compared to the RBM bands of the Raman spectra taken from SWNTs on a silicon oxide substrate, the RBM bands taken from suspended SWNTs exhibit narrower linewidths and stronger signals. Before the deconvolution of the RBM bands with the instrumental function, RBM linewidths (FWHM) down to $3cm^{-1}$ are observed from suspended SWNTs, while RBM linewidths down to $5cm^{-1}$ are observed from the SWNTs on a silicon oxide substrate [5]. After the deconvolution of the RBM bands with the instrumental function, a RBM linewidth down to $2cm^{-1}$ is obtained from suspended SWNTs and an RBM linewidth down to $3cm^{-1}$ is observed from the SWNTs on a silicon oxide substrate [5], .

Table 4-1 summarizes the RBM frequencies (ω_{RBM}) and the normalized I_{AS} / I_S intensity ratio obtained from suspended SWNTs on high-density samples, as shown in Figure 3-4 (a) and low-density samples as shown in Figure 3-4 (b). Suspended SWNTs from high-density samples have a higher probability of being bundled or being resonant with non-E_{ii} transitions, such as E_{12}, than suspended SWNTs from low-density samples, since the SWNTs are not well aligned and closer to each other. As the resonance window is not known for suspended SWNTs, E_{ii} values can only be estimated as follows. If the normalized I_{AS} / I_S intensity ratio is small or large, E_{ii} is approximately equal to the E_{laser} - E_{ph} or E_{laser} + E_{ph}, respectively. Errors in E_{ii} are due to the assumption that the resonance window of suspended SWNT is smaller than the resonance window of SWNTs on a silicon oxide substrate, which is 8meV. Figure 4-5 shows I_{AS} and I_S of SWNTs on a silicon oxide substrate, which can be used to calculate the normalized I_{AS} / I_S intensity ratio as a function of E_{laser} and

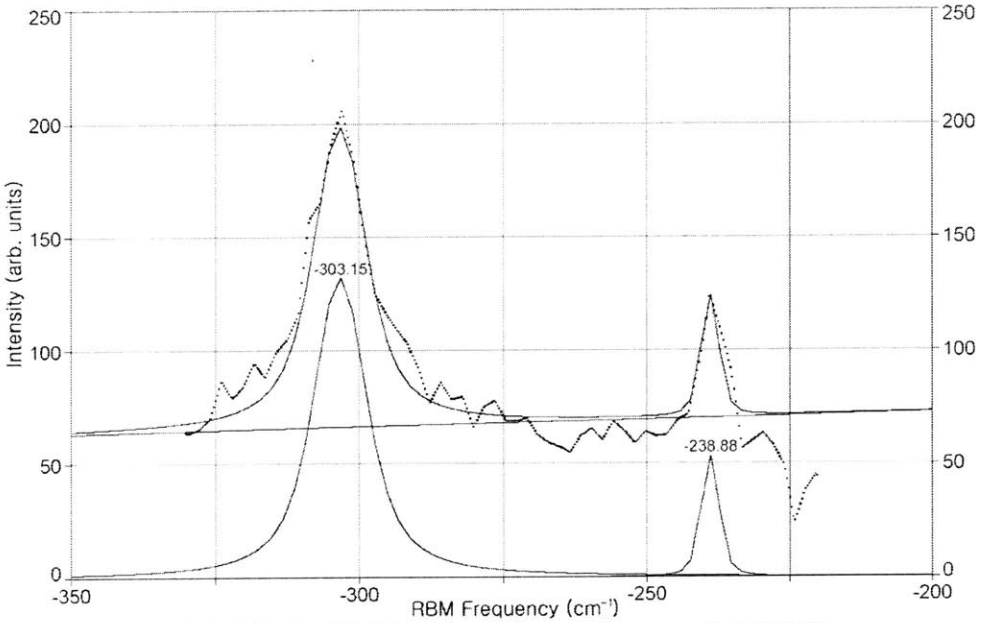

(a) Anti-Stokes RBM mode spectrum of a suspended SWNT

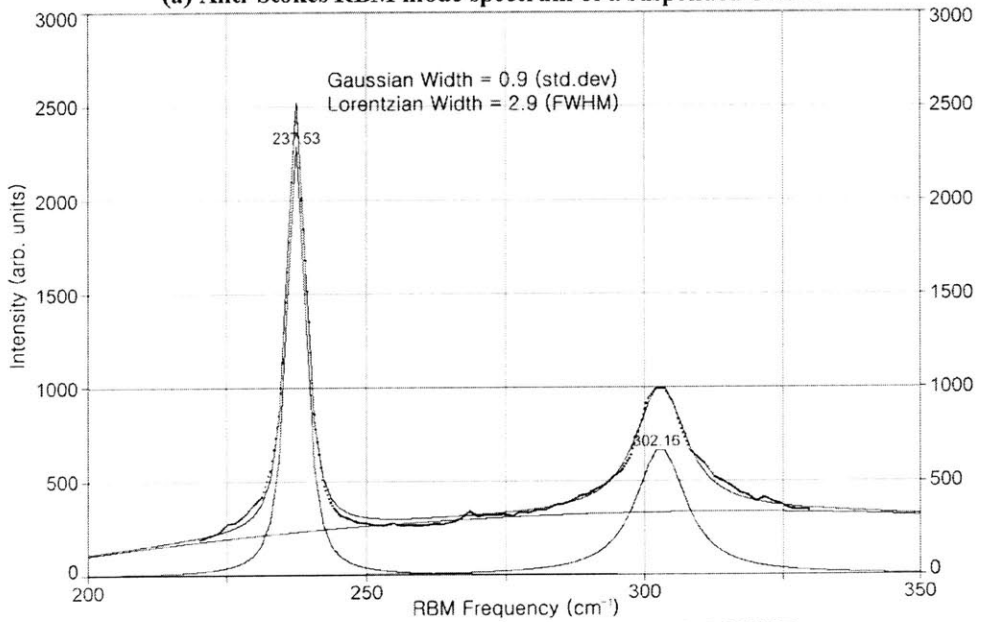

(b) Stokes RBM mode spectrum of a suspended SWNT

Figure 4-3: The anti-Stokes and Stokes RBM bands of the Raman spectrum taken simultaneously from a suspended SWNT using $E_{laser} = 1.58$eV, demonstrating the ability to obtain data with a low anti-Stokes to Stokes intensity ratio.

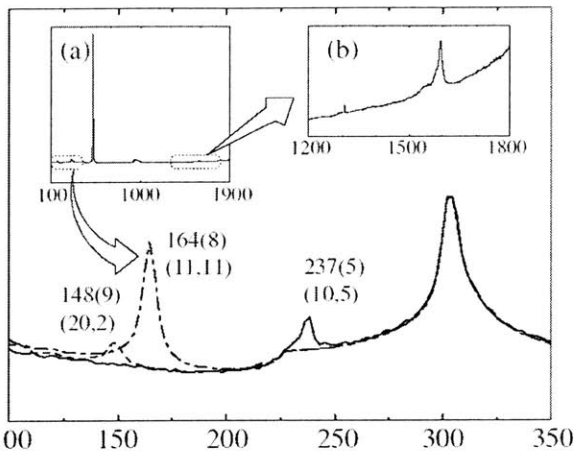

Figure 4-4: Raman spectra from three different spots on the Si substrate with E_{laser}=1.58eV, showing only one resonant nanotube and one RBM frequency for each of 3 spots. The RBM frequencies (widths) and (n,m) assignment for each resonant SWNT are displayed. Figure taken from [9].

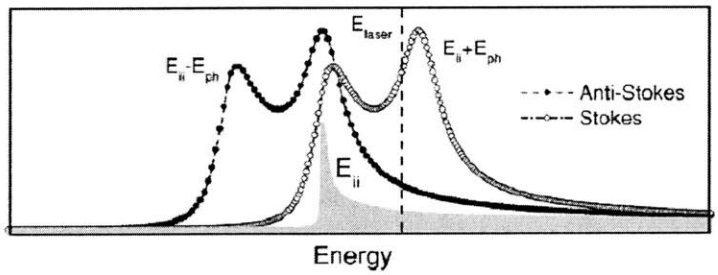

Figure 4-5: The anti-Stokes and Stokes intensity of the RBM band of SWNTs on a Si/SiO_2 substrate as a function of E_{laser} (the vertical line) and E_{ii}. The resonance window I_S = 8meV. Figure taken from [7].

E_{ii} [7]. By comparing the calculated I_{AS} / I_S to the experimental I_{AS} / I_S, the range of possible E_{ii} can be obtained. However, as the resonance window is not known for suspended SWNTs, this range of E_{ii} is used to estimate the error.

Table 4.1: RBM and estimated E_{ii} values based on the anti-Stokes and Stokes intensity ratios obtained from suspended SWNTs. The error for ω_{RBM} is $\pm 0.5 \mathrm{cm}^{-1}$ and the error for normalized I_{AS} / I_S is $\pm 20\%$.

Sample Density[a]	$\omega_{RBM}(\mathrm{cm}^{-1})$	Normalized I_{AS} / I_S	E_{laser}(eV)	E_{ii}(eV)
High	174	1.6	2.41	>2.41
High	176	0.77	2.41	<2.41
High	177	1.9	2.41	2.43±0.03
High	180	1.7	2.41	>2.41
High	186	0.90	2.41	<2.41
High	195	2.4	2.41	2.43±0.02
High	221	1.2	2.41	>2.41
High	270	2.1	2.41	2.44±0.02
High	205	1.3	1.58	>1.58
High	208	3.5	1.58	1.61±0.02
High	210	0.93	1.58	<1.58
High	217	0.20	1.58	1.55±0.01
High	224	0.45	1.58	1.55±0.02
High	227	0.33	1.58	1.55±0.01
High	237	0.28	1.58	1.55±0.01
High	249	0.30	1.58	1.55±0.01
High	253	0.41	1.58	1.55±0.01
High	267	0.22	1.58	1.54±0.01
High	268	3.3	1.58	1.61±0.02
Low	206	0.52	1.58	1.55±0.02
Low	216	0.42	1.58	1.55±0.01
Low	226	0.35	1.58	1.55±0.01
Low	238	0.092[b]	1.58	1.55±0.01
Low	267	4.0	1.58	1.61±0.02

[a]SEM images of high-density samples are shown in Figure 3-4 (a) and SEM images of low-density samples are shown in Figure 3-4 (c)

[b]Observation of an I_{AS}/I_S ratio as low as 0.092 is not possible with a resonance window of 8meV.

Chapter 5

Discussion

The normalized anti-Stokes and Stokes intensity ratio I_{AS}/I_S of the Radial Breathing Mode feature of the Raman spectra is used to estimate the electronic transition energies (E_{ii}) in the electronic bands of SWNTs. The RBM frequency of the Raman spectra provides good estimates for the diameter of the SWNT. These estimates have been used to make the (n,m) assignment of SWNTs on a Si/SiO_2 substrate [7] and SDS-wrapped SWNTs [6]. The RBM frequencies of the inner walls of DWNTs are used to make (n,m) assignments for these SWNTs [21]. The photoluminescence data from SDS-wrapped SWNTs [1] and suspended SWNTs on silicon pillars [17] also give valuable information about the E_{ii} values and are also used to make (n,m) assignments. In this chapter, side-by-side comparisons are made between the Raman data of suspended SWNTs and other published data, as mentioned above.

The ω_{RBM} and estimated E_{ii} measured in this thesis on suspended SWNTs are plotted in Figure 5-1 along with a Kataura plot based on tight-binding model [13]. The ω_{RBM} of the tight-binding model is calculated by $\omega_{RBM}(\mathrm{cm}^{-1}) = 248/d_t$, where d_t is the diameter of the SWNT in nm, and $\gamma_0 = 2.9\mathrm{eV}$ [25]. The data points from suspended SWNTs clearly fall in one of the E_{ii} bands. However, the spread in ω_{RBM} from suspended SWNTs in the E_{22}^S band appear to be a lot greater than what the tight-binding model predicts, possibly due to the small diameter of the SWNTs and the inaccuracies in their model in the limit of small diameter SWNTs [7].

The ω_{RBM} and estimated E_{ii} measured in this thesis on suspended SWNTs are

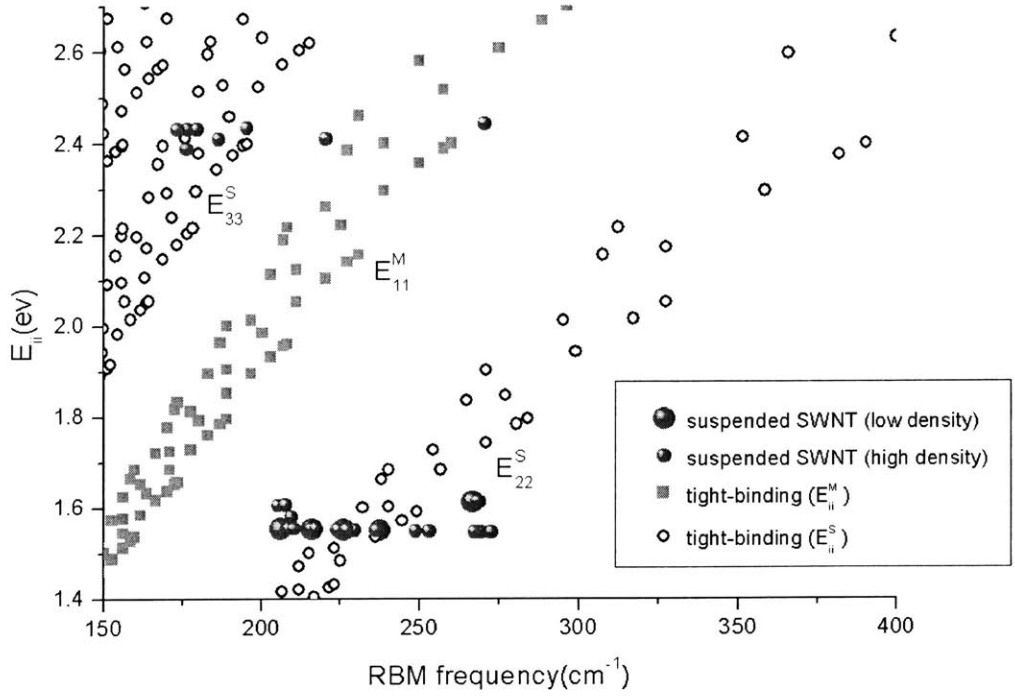

Figure 5-1: The ω_{RBM} and estimated E_{ii} obtained experimentally for suspended SWNTs are plotted against the tight-binding model predictions.

plotted in Figure 5-2 along with a Kataura plot based on the symmetry-adapted non-orthogonal tight-binding model using $2s$ and $2p$ electrons of carbon [22]. The ω_{RBM} of the non-orthogonal tight-binding model is calculated by $\omega_{RBM}(\mathrm{cm}^{-1}) = 248/d_t(\mathrm{nm})$. The spread in ω_{RBM} from suspended SWNTs at a given laser line is more consistent with the non-orthogonal tight-binding model predictions than the tight-binding model predictions, but the center of the ω_{RBM} distribution at a given laser line is in poor agreement with the non-orthogonal tight-binding model predictions. This might suggest that the non-orthogonal tight-binding model has over-optimized the parameters and a more accurate model should take an approach somewhere between that taken by the tight binding model and the non-orthogonal tight-binding model.

In Figure 5-3, the ω_{RBM} and the estimated E_{ii} obtained experimentally from suspended SWNTs are compared to the ω_{RBM} measured from the inner walls of DWNTs using many laser lines [21]. The open squares are the ω_{RBM} measured from the inner walls of DWNTs at a given E_{laser}. The dark squares represent the strongest

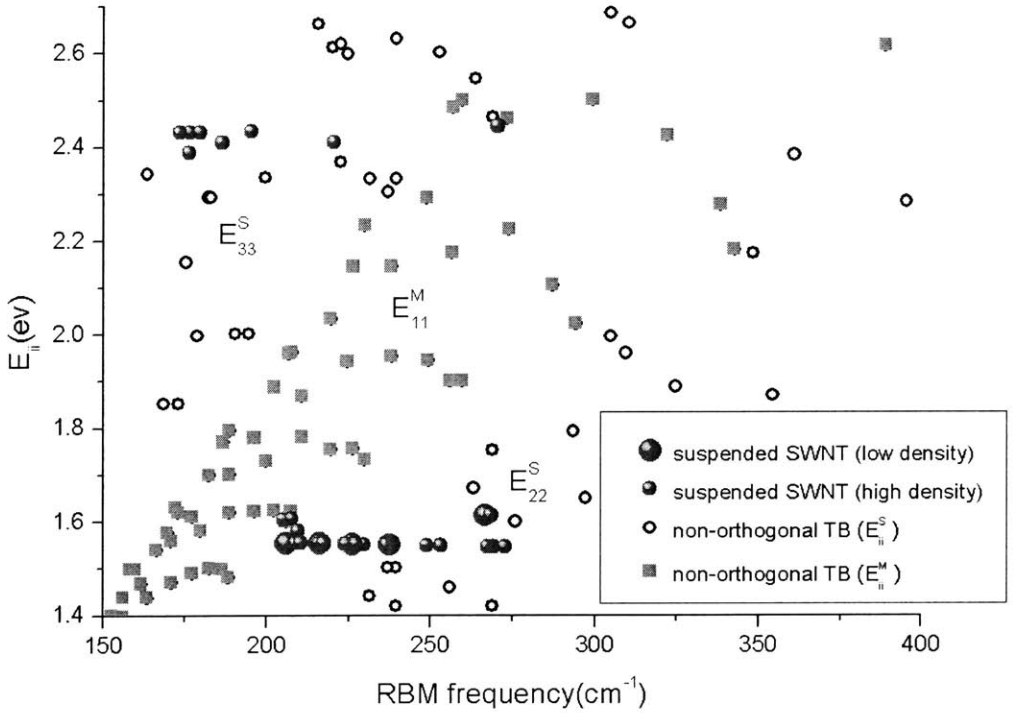

Figure 5-2: The ω_{RBM} and estimated E_{ii} obtained experimentally for suspended SWNTs are plotted against the non-orthogonal tight-binding model predictions.

and the next strongest peak in the spectrum taken at a given E_{laser}. Only ω_{RBM} values corresponding to RBM peaks with intensities greater than about 30% of the intensity of the second strongest peak in each spectrum are plotted. The dotted lines denote the approximate top and bottom envelopes and the center line of the E_{22}^S band. The bottom envelope is not as apparent as the top envelope.

Unfortunately, the laser lines used for the inner walls of DWNTs do not match the laser lines used for the suspended SWNTs. However, a trend can be clearly seen: the ω_{RBM} and estimated E_{22}^S measured from suspended SWNTs span the envelope of the E_{22}^S band measured from the inner walls of DWNTs. Moreover, the suspended SWNT with $\omega_{RBM} = 267\text{cm}^{-1}$ and $E_{ii} = 1.61\text{eV}$ can be correlated with the inner wall of a DWNT with $\omega_{RBM} = 267\text{cm}^{-1}$, $E_{ii} = 1.60\text{eV}$, and (n,m) = (11,1) or with the inner wall of a DWNT with $\omega_{RBM} = 269\text{cm}^{-1}$, $E_{ii} = 1.60\text{eV}$, and (n,m) = (9,4). The (n,m) assignment of the inner walls of DWNTs is made based on $\omega_{RBM}(\text{cm}^{-1}) = 248/d_t(\text{nm})$ [21].

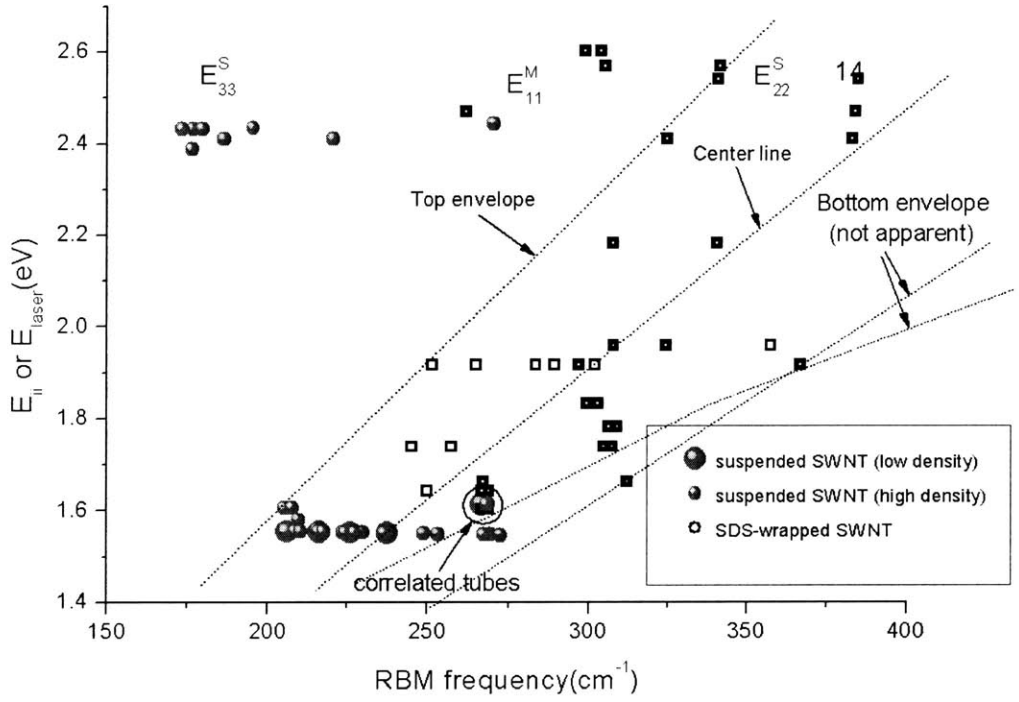

Figure 5-3: The ω_{RBM} and estimated E_{ii} values obtained experimentally for suspended SWNTs are compared to the ω_{RBM} measured from the inner walls of DWNTs using many laser lines. Thick black squares indicate the strongest and the next strongest peaks in the spectrum taken at a given E_{laser}.

Table 5.1: A possible assignment of the suspended SWNTs based on the SDS-wrapped SWNT data.

Suspended SWNT		SDS-wrapped SWNT		(n,m)
ω_{RBM}	E_{22}^{S}(eV)	ω_{RBM}	E_{22}^{S}(eV)	
206	1.55±0.02	203	1.53	(9,8)
216	1.55±0.01	216	1.57	(9,7)
226	1.55±0.01	225	1.58	(10,5)
238	1.55±0.01[a]	237	1.55	(12,1)

[a]The normalized I_{AS}/I_{S} is 0.092 and indicates that E_{22}^{S} is very close to 1.55eV. See Figure 4-5.

In Figure 5-4, the ω_{RBM} and the estimated E_{ii} experimentally observed from suspended SWNTs are plotted with the experimental ω_{RBM} and E_{ii} obtained from SDS-wrapped SWNTs [6]. The short dashed lines connecting a few points indicate the identified (2n+m) families for semiconducting SWNTs and the family numbers are shown. The long dashed lines are the envelope of the E_{22}^{S} band of the SDS-wrapped SWNTs. Again, the ω_{RBM} and estimated E_{ii} from suspended SWNTs follow the trend from SDS-wrapped tubes well. Especially, the data points from suspended SWNTs from the low-density samples are very close to some of the data points from the SDS-wrapped SWNTs. Some of the data points from suspended SWNTs on the high-density samples deviate from the identified E_{ii} bands of the SDS-wrapped SWNTs. This suggests that some SWNTs on the high-density samples are resonant with non-E_{ii} transitions. Furthermore, it is difficult to correlate the E_{11}^{M} and E_{33}^{S} points from the high-density sample with points from the SDS-wrapped SWNTs. This suggests that ω_{RBM} and E_{ii} values might shift due to the bundling of suspended SWNTs and/or wrapping SWNTs with SDS.

Table 5-1 shows a possible (n,m) assignment of suspended SWNTs based on the (n,m) assignment of SDS-wrapped SWNTs. Only the data points from the low-density samples are considered, since the suspended SWNTs from the high-density samples have a greater probability of being bundled or being resonant with non-E_{ii} transitions. In general, good agreement in ω_{RBM} can be found, whereas the E_{22}^{S} values of suspended SWNTs, in general, appear to be lower by 0meV to 30meV.

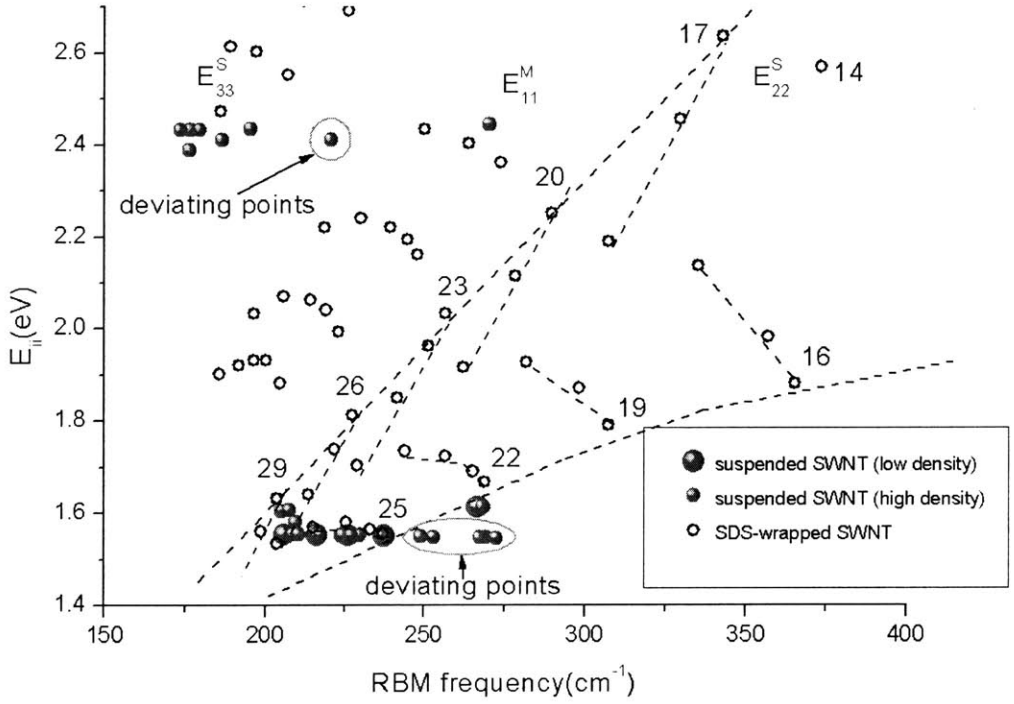

Figure 5-4: The ω_{RBM} and estimated E_{ii} values obtained experimentally for suspended SWNTs in comparison to SDS-wrapped SWNTs. Points outside the envelope are indicated (see text).

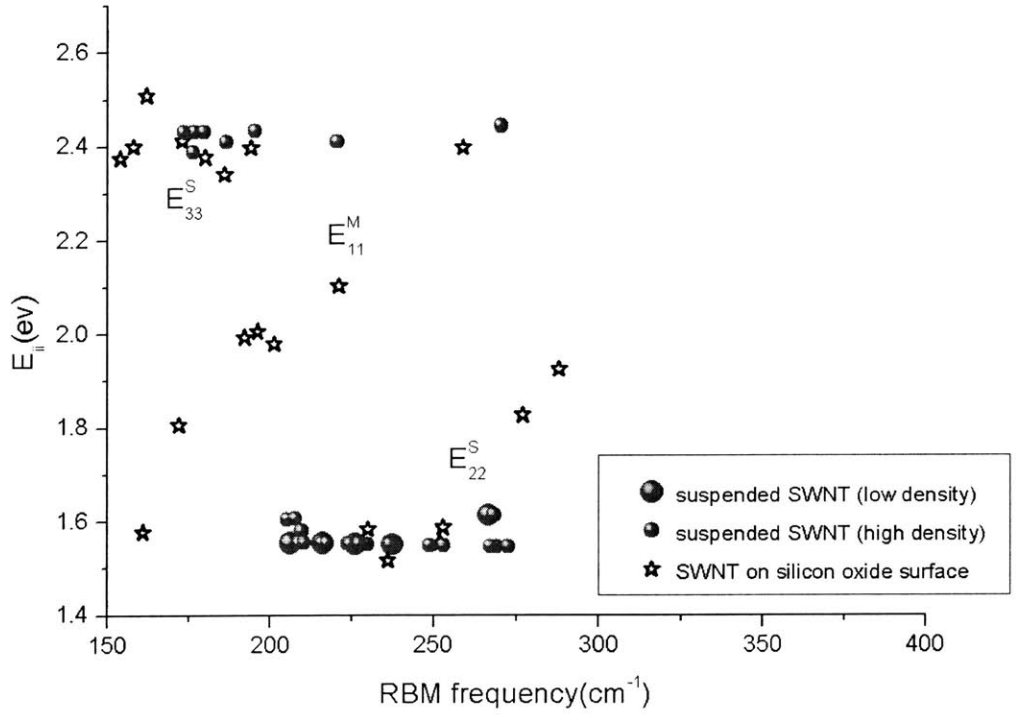

Figure 5-5: A comparison between the ω_{RBM} and estimated E_{ii} values for suspended SWNTs and for SWNTs on silicon oxide substrate.

In Figure 5-5, the ω_{RBM} and estimated E_{ii} values obtained experimentally for suspended SWNTs are plotted in comparison to the corresponding ω_{RBM} and E_{ii} values from the anti-Stokes to Stokes intensity ratio analysis carried out for SWNTs on a Si/SiO_2 surface [7]. Although the center of the ω_{RBM} distribution at a given E_{ii} seems to agree, the spread in the ω_{RBM} distribution at a given E_{ii} is significantly different. Thus, a complete set of data points from SWNTs on a Si/SiO_2 surface and/or suspended SWNTs would be required to make one to one assignments.

In Table 5-2, a comparison of the E_{22}^S values of the suspended SWNTs is made with the E_{22}^S values obtained from the photoluminescence from the suspended SWNTs on silicon pillars [16]. Although, no reliable assignment can be made, even though the E_{22}^S values from both works are obtained from suspended SWNTs, the best assignment is made by giving more weight to the ω_{RBM} values. Since there are not enough points from each work, it might not be feasible to make a reliable one-to-one assignment at present. As shown in Figure 4-5, Raman spectroscopy is expected to discover few

Table 5.2: The E_{22}^S values obtained from Raman spectroscopy and photoluminescence on suspended SWNTs.

Photoluminescence		Raman		(n,m)[a]
ω_{RBM}[b]	E_{22}^S(eV)	ω_{RBM}	E_{22}^S(eV)	
196	1.566	-	-	(12,5)
201	1.640	-	-	(13,3)
203	1.550	206	1.55±0.02	(9,8)
213	1.651	-	-	(10,6)
215	1.588	216	1.55±0.01	(9,7)
225	1.601	226	1.55±0.01	(10,5)
231	1.593	-	-	(11,3)
234	-	238	1.55±0.01	(12,1)

[a]Taken from [16].

[b]ω_{RBM} is calculated by the following formula: $\omega_{RBM}(\text{cm}^{-1}) = 225.5/d_t(\text{nm}) + 12.5$ [1].

SWNTs with $E_{ii} > E_{laser}$. This could be the reason why the E_{22}^S values from Raman spectroscopy cannot match E_{22}^S values greater than 1.58eV from photoluminescence.

Good agreement in the trend in the ω_{RBM} and E_{ii} values obtained experimentally from suspended SWNTs and that obtained experimentally from the inner walls of DWNTs and SDS-wrapped SWNTs was found, and some preliminary (n,m) assignments of suspended SWNTs could be made, based upon the (n,m) assignments of the inner walls of DWNTs and SDS-wrapped SWNTs. However, this work is limited in the following way. First, the available laser lines are limited and, thus, the suspended SWNT data are not complete and the E_{ii} values are only estimates. Second, the number of data points obtained from the low-density samples is very limited and there is no guarantee that these are actually from individual suspended SWNTs rather than from bundles of a small number of SWNTs.

In future work, Raman spectroscopy with a tunable laser would be desirable. Such experiments would enable the precise measurement of the E_{ii} values and would allow us to perform resonance Raman spectroscopy with a greater number of (n,m) species of suspended SWNTs. Furthermore the resonance window would tell us whether the SWNTs under inspection are bundled or are individual suspended SWNTs. The challenges would be the lower efficiency and the high cost of tunable Raman systems.

However, the greatly enhanced Raman signal from suspended SWNTs might allow resonance Raman spectroscopy to be carried out in a much more quantitative way with such tunable Raman systems.

Bibliography

[1] Sergei M. Bachilo, Michael S. Strano, Carter Kittrell, Robert H. Hauge, Richard E. Smalley, and R. Bruce Weisman. Structure-assigned optical spectra of single-walled carbon nanotubes. *Science, 298, 2361*, 2002.

[2] Jien Cao, Qian Wang, Dunwei Wang, and Hongjie Dai. Suspended carbon nanotube quantum dots with two gates. *unpublished*, 2003.

[3] S. G. Chou, H. B. Ribeiro, A. P. Santos, D. Nazich, Ge. G. Samsondize, C. Fantini, M. A. Pimenta, A. Jorio, F. Plentz Filho, M. S. Dresselhaus, and G. Dresselhaus. Optical measurements of gt-dna wrapped carbon nanotubes hybrids. *unpublished*, 2004.

[4] M. S. Dresselhaus, G. Dresselhaus, and Ph. Avouris. *Carbon Nanotubes: Synthesis, Structures and Applications.* Springer, Berlin, 2001.

[5] M.S. Dresselhaus, G. Dresselhaus, A. Jorio, A.G. Souza Filho, and R. Saito. Raman spectroscopy on isolated single wall carbon nanotubes. *Carbon, 40, 2043*, 2002.

[6] C. Fantini, A. Jorio, M. Souza, A. J. Mai Jr., M. S. Strano, M. S. Dresselhaus, and M. A. Pimenta. Optical transition energies for carbon nanotubes from resonant raman spectroscopy: Environment and temperature effects. *unpublished*, 2004.

[7] A. G. Souza Filho, S. G. Chou, Ge. G. Samsonidze, G. Dresselhaus, M. S. Dresselhaus, Lei An, J. Liu, Anna K. Swan, M. S. Unlu, and B. B. Goldberg. Stokes and

anti-stokes raman spectra of small-diameter isolated carbon nanotubes. *Phys. Rev. B, 69, 115428*, 2004.

[8] A. Jorio, M. A. Pimenta, A. G. Souza Filho, R. Saito, G. Dresselhaus, and M. S. Dresselhaus. Characterizing carbon nanotube samples with resonance raman scattering. *New J. Phys., 5, 139.1-139.17*, 2003.

[9] A. Jorio, R. Saito, J. H. Hafner, C. M. Lieber, M. Hunter, T. McClure, G. Dresselhaus, and M. S. Dresselhaus. Structural (n,m) determination of isolated single-wall carbon nanotubes by resonant raman scattering. *Phys. Rev. Letts., 86, 6, 1118*, 2001.

[10] A. Jorio, R. Saito, T. Hertel, R.B. Weisman, G. Dresselhaus, and M.S. Dresselhaus. Carbon nanotube photophysics. *MRS Bulletin, Apr, 2004, 276*, Apr, 2004.

[11] Ernesto Joselevich and Charles M. Lieber. Vectorial growth of metallic and semiconducting single-wall carbon nanotubes. *Nano Lett., 2, 10, 1137*, 2002.

[12] Akinobu Kanda, Youiti Ootuk, Kazuhito Tsukagoshi, and Yoshinobu Aoyagi. Growth of suspended carbon nanotube networks on 100-nm-scale silicon pillars. *Appl. Phys. Lett., 81, 12*, 2002.

[13] H. Kataura, Y. Kumazawa, Y. Maniwa, I. Umezu, S. Suzuki, Y. Ohtsuka, and Y. Achiba. Optical properties of single-wall carbon nanotubes. *Synth. Metals, 103, 2555*, 1999.

[14] Yoshihiro Kobayashi, Takayuki Yamashita, Yuko Ueno, Osamu Niwa, Yoshikazu Homma, and Toshio Ogino. Extremely intense raman signals from single-walled carbon nanotubes suspended between si nanopillars. *Chem. Phys. Lett., 386, 153*, 2004.

[15] Jing Kong, Hyongsok T. Soh, Alan M. Cassell, Calvin F. Quate, and Hongjie Dai. Synthesis of individual single walled carbon nanotubes on patterned silicon wafers. *Nature, 395, 29*, 1998.

[16] J. Lefebvre, J.M. Fraser, Y. Homma, and P. Finnie. Photoluminescence from single-walled carbon nanotubes: a comparison between suspended and micelle-encapsulated nanotubes. *Appl. Phys. A, 78, 1107*, 2004.

[17] J. Lefebvre, Y. Homma, and P. Finnie. Bright band gap photoluminescence from unprocessed single-walled carbon nanotubes. *Phys. Rev. Letts., 90, 217401*, 2003.

[18] Jie Liu, Shoushan Fan, and Hongjie Dai. Recent advances in methods of forming carbon nanotubes. *MRS Bulletin, Apr, 2004, 244*, 2004.

[19] Michael J. O'Connell, Sergei M. Bachilo, Chad B. Huffman, Valerie C. Moore, Michael S. Strano, Erik H. Haroz, Kristy L. Rialon, Peter J. Boul, William H. Noon, Carter Kittrell, Jianpeng Ma, Robert H. Hauge, R. Bruce Weisman, and Richard E. Smalley. Band gap fluorescence from individual single-walled carbon nanotubes. *Science, 297, 593*, 2002.

[20] Takahito Ono, Hidetoshi Miyashita, and Masayoshi Esashi. Electric-field-enhanced growth of carbon nanotubes for scanning probe microscopy. *Nanotechnology, 13, 62*, 2002.

[21] R. Pfeiffer, H. Kuzmany, Ch. Kramberger, Ch. Schaman, T. Pichler, H. Kataura, Y. Achiba, J. Kurti, and V. Zolyomi. Unusual high degree of unperturbed environment in the interior of single-wall carbon nanotubes. *Phys. Rev. B, 90, 225501*, 2003.

[22] Valentin N Popov. Curvature effects on the structural, electronic and optical properties of isolated single-walled carbon nanotubes within a symmetry-adapted non-orthogonal tight-binding model. *New J. Phys., 6, 17*, 2004.

[23] A. M. Rao, E. Richter, Shunji Bandow, Bruce Chase, P. C. Eklund, K. A. Williams, S. Fang, K. R. Subbaswamy, M. Menon, A. Thess, R. E. Smalley, G. Dresselhaus, and M. S. Dresselhaus. Diameter-selective raman scattering from vibrational modes in carbon nanotubes. *Science, 275, 187*, 1997.

[24] R. Saito, G. Dresselhaus, and M. S. Dresselhaus. *Physical Properties of Carbon Nanotubes.* Imperial College Press, 1999.

[25] R. Saito, G. Dresselhaus, and M. S. Dresselhaus. Trigonal warping effect of carbon nanotubes. *Phys. Rev. B, 61, 4, 2981*, 2000.

[26] Yuegang Zhang, Aileen Chang, Jien Cao, Qian Wang, Woong Kim, Yiming Li, Nathan Morris, Erhan Yenilmez, Jing Kong, and Hongjie Dai. Electric-field-directed growth of aligned single-walled carbon nanotubes. *Appl. Phys. Lett., 79, 19*, 2001.